Natural ELF Electromagnetic Pulses

A.P. Nickolaenko

An interest towards monitoring the natural electromagnetic pulse radio signals re-appeared recently stimulated by the attempts of location the distant powerful lightning strokes that cause optical emissions in the upper atmosphere. Such a luminous structure over a thunderstorm cell may reache the 95 km altitude. Optical events were classified as 'red sprites', 'elves', and 'blue jets', see [1-3] and reference therein. The observations were performed over the USA territory, and the co-ordinates of causative strokes were established with the National Lightning Detection Network. To cover a wider territory, an application of the Schumann resonance frequency range had been suggested, namely, the frequencies from a few Hz to a hundred Hz [4]. The slow tail technique may be applied as well at the distances to a few thousands km, see [5] and reference therein. Slow tail atmospherics are observed at the frequencies from a few hundred to a few thousand Hz. Both the measurement techniques are not new, these were developed and used actively in 60s-70s. A zero order mode or TEM wave propagates in the Earth-ionosphere waveguide at the frequencies below 1.6-1.7 kHz. The first transverse resonance occurs at the above frequency [6], the particular value depends on the ambient day- or night-time propagation conditions.

The wave attenuation factor is small below the 100 Hz frequency, enabling a radio wave to travel around the Earth's circumference. The global or Shumann resonance (SR) is observed then. When the frequency increases, the wave absorption grows, and the 'round-the-world' waves become so small that the resonance vanish, and the spectra become smooth. This was one of a reasons why the Q-bursts in the SR range and the slow tail atmospherics that are observed at higher frequencies were treated separately.

The goal of the present study is an analysis of the model solution within the whole the extremely low frequency (ELF) band. We apply a well-known frequency domain solution for the wave travelling in the spherical Earth-ionosphere cavity. The time dependent field components are obtained with the numerical Fourier transform. Within such an approach, any further development of the known theory is unnecessary, and the field distribution over the frequency-distance plane are obtained from the unified positions.

We describe ELF spectral components of an electromagnetic wave using the mode theory developed for the spherical Earth-ionosphere waveguide [7-9]:

$$E_r = \frac{i\nu(\nu+1)}{\omega} \cdot \frac{M_c(\omega)}{4a^2h\varepsilon} \cdot \frac{P_\nu\big[\cos(\pi-\theta)\big]}{\sin \pi\nu} \tag{1}$$

$$H_\varphi = -\frac{M_c(\omega)}{4ah} \cdot \frac{P_\nu^1\big[\cos(\pi-\theta)\big]}{\sin \pi\nu} \tag{2}.$$

Here $\nu(\omega)$ is the propagation constant of the ELF radio wave, ω is the circular frequency, $M_c(\omega)$ is the current moment of the source, θ is the angular distance between the source and observer, a is the Earth's radius, h is the effective height of the ionosphere, ε is the dielectric constant of the free space, $P_\nu(x)$ and $P_\nu^1(x)$ are the Legendre and associated Legendre functions.

We specify the following model parameters: $a = 6.4$ Mm, $h = 60$ km, and $M_c = const = 10^8$ Am. In other words, the current moment of the source in the time-domain is the Dirac's delta-pulse. The single zero-order mode or TEM wave propagates in the frequency range between a few Hz to approximately 2 kHz. When the condition $kh > 1$ is satisfied at higher frequencies (here k is the free space wavenumber and h is the effective height of the ionosphere), the first mode electric and magnetic waves appear which are not treated in the present work.

One has to define an appropriate $\nu(f)$ dependence before computing the fields. Obtaining such a dependence is a separate problem: the eigen-values are sought for a radial operator describing propagation of the electromagnetic wave between ground and the ionosphere. In this context, the Earth is usually supposed to be a

perfectly conducting sphere, while the ionosphere is characterised by an effective height and surface impedance pertinent to a diffusive plasma boundary [7-9]. Rigorous but much more complicated approaches could be used as well, see e.g. [10]. We apply the following heuristic dependence

$$\nu(f) = \nu_1 - i\nu_2 = (f-2)/6 - i \cdot f /100 \qquad (3).$$

The above dependence is based on the statistical analyses of the cross-spectra obtained in the SR range for two widely separated observatories [9]. Equation (3) had been already applied when modelling the ELF fields, [11-13], still, its validity at the frequencies above the SR band should be demonstrated via comparison with other models or with the experimental data. The last are rare unfortunately.

To justify our model (3), we use the results [14], obtained for an exponential conductivity profile of the atmosphere. Suppose the profile is characterised by a single altitude scale factor ζ:

$$\sigma(z) = 2 \cdot \pi \cdot \varepsilon \cdot \exp[\,(z-G)/\zeta\,] \qquad (4).$$

Here z is the altitude above the ground, ζ is the height scale factor, and G is the 'normal' altitude. This last is the altitude, where the conductivity and displacement currents become equal at the 1 Hz frequency.

The zero or TEM mode propagation constant $\nu(f)$ is found for such a profile from the expression [14]:

$$\nu(\nu+1) = (ka)^2 \cdot \frac{h_1 + i\zeta\pi/2}{h_o - i\zeta\pi/2} \qquad (5)$$

with the following approximate solution that is valid when $\zeta << h_o, h_1$:

$$\nu_1 = Re\nu = ka \cdot (h_1/h_o)^{1/2} \qquad (6a)$$

and

$$\nu_2 = Im\nu = ka \cdot \zeta \cdot (\pi/4) \cdot (1/h_1 + 1/h_o) \qquad (6b).$$

Here $h_o = G + \zeta \cdot \ln(f)$ is the altitude where the conductivity and displacement currents become equal for the particular frequency f, and $h_1 = h_o - 2\zeta \cdot \ln(2k\zeta)$ is the height of the diffusion of the magnetic field component into the ionosphere.

The above formulas were obtained for the plane waveguide. Still, these are valid for the curved boundaries as well, provided the radius of curvature is much greater than the skin-depth of the electromagnetic wave in the ionosphere [15]. The problem for the spherical Earth was analysed in [16], and it was demonstrated that the above equations remain valid for any realistic model of the Earth-ionosphere cavity.

We depict the $\nu(f)$ dependence computed for two exponential conductivity profiles (curves 1 and 2) and for the heuristic formula (curve 3) in Fig.1. The upper frame in the figure shows the function $Re\{\nu(f)\}$. The lower one demonstrates the frequency variations of the wave attenuation factor $-Im\nu\{(f)\}$. Three curves are shown in each chart. The curve labelled with 1 represents the ambient night conditions with the vertical conductivity profile having the scale factor $\zeta = 2.5$ km and the normal altitude $G = 50$ km. Label 2 marks the propagation constant calculated for the ambient day conditions with a smaller normal altitude $G = 38.8$ km and increased scale factor $\zeta = 3.4$ km, see [15]. The curve 3 is the heuristic linear $\nu(f)$ approximation (3) applied in this work.

Comparing plots in Fig.1, we conclude that the dispersion relation (3) is in accord with the exponential conductivity profile of the atmosphere. There is a systematic deviation in the ELF phase velocity that does not exceed the 15% level in the whole ELF range, while the attenuation factor of equation (3) lies between reasonable ambient day- and night-time profiles. Hence, the simple equation (3) may be used when modelling the zero mode propagation in the Earth-ionosphere duct.

We prefer the equation (3) since:
- it is of the simplest form,
- it extends the experimental results of the cross-spectral SR data to the whole ELF range, and
- it is rather close to the dependencies obtained for the exponential conductivity profile of the atmosphere

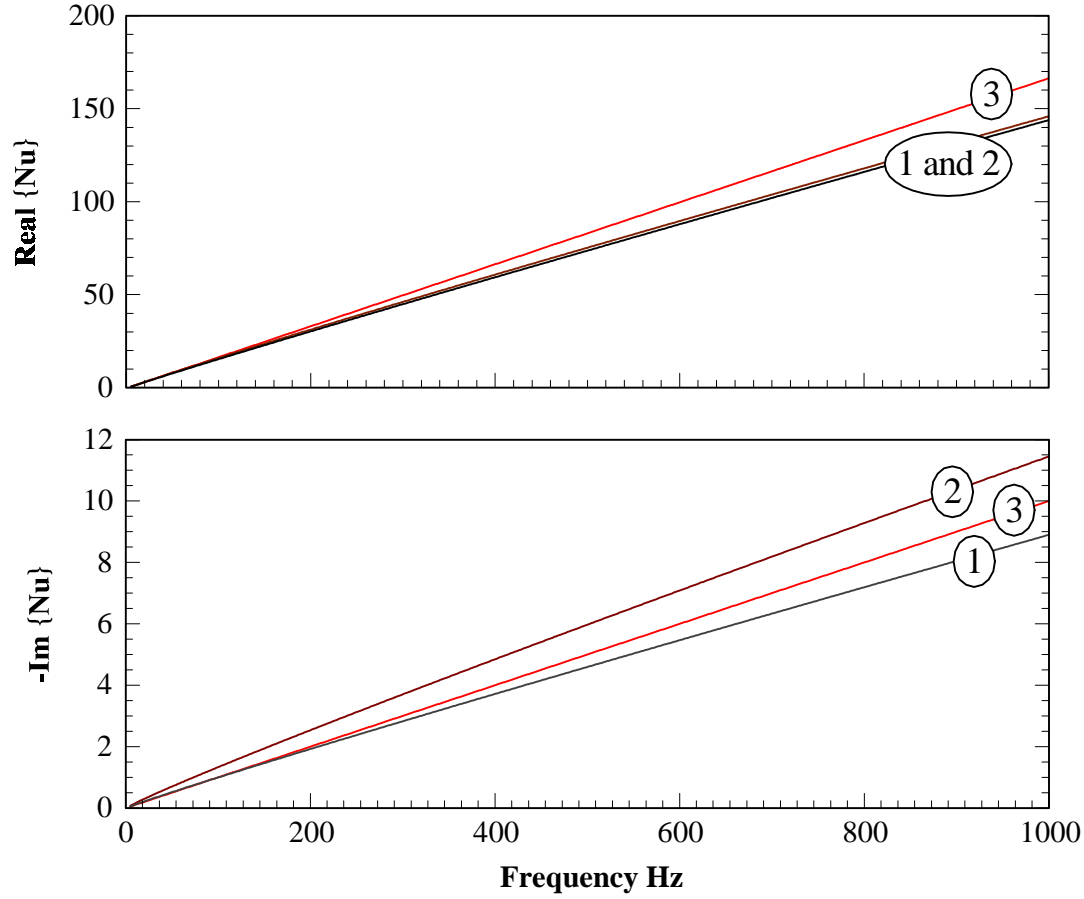# Propagation Constant $\nu(f)$

Fig. 1. Comparison between the heuristic $\nu(f)$ dependence (3) with those computed for the exponential conductivity profiles of the atmosphere in ambient day (1) and night (2) conditions.

We confine ourselves to computing the vertical electric field component in the present paper. Obtaining similar results for the horizontal magnetic field is rather straightforward.

When computing the field, we divide the frequency range into three strips, and use different representation for the Legendre function $P_\nu(-x)$ within these strips. In the frequency range below 150Hz, we apply the zonal harmonic series representations (ZHSR) [9, 17] with an accelerated convergence:

$$P_\nu\left[\cos(\pi-\theta)\right]=-\frac{\sin\pi\nu}{\pi}\sum_{n=0}^{\infty}\frac{(2n+1)\cdot P_n(\cos\theta)}{n(n+1)-\nu(\nu+1)} \qquad f\leq150 \qquad (7).$$

The 'trigonometric' asymptotic expansions are used at frequencies above the SR band:

$$P_\nu\left[\cos(\pi-\theta)\right]=\left(\frac{2}{\pi(\nu+1/2)\sin\theta}\right)^{1/2}\cos\left[(\nu+1/2)(\pi-\theta)-\pi/4\right] \qquad 150<f\leq1700 \qquad (8).$$

Equations with single direct wave from the source are used when $f > 1.7$ kHz:

$$\frac{P_\nu\left[\cos(\pi-\theta)\right]}{\sin \pi \nu} = i\left(\frac{2}{\pi(\nu+1/2)\sin\theta}\right)^{1/2} \exp\left\{-i\left[(\nu_1+1/2)\theta - \pi/4\right] - \nu_2\theta\right\} \qquad f > 1700 \qquad (9).$$

Equation (9) does not describe characteristic amplitude variations of the field along the distance when the observer approaches to the source antipode. But, such an effect becomes pronounced in a close (500-1000 km) vicinity of the antipode because the attenuation of the radio waves is high. Hence, the above formulas describe the main features of the ELF field in the range from 1 to 20 Mm
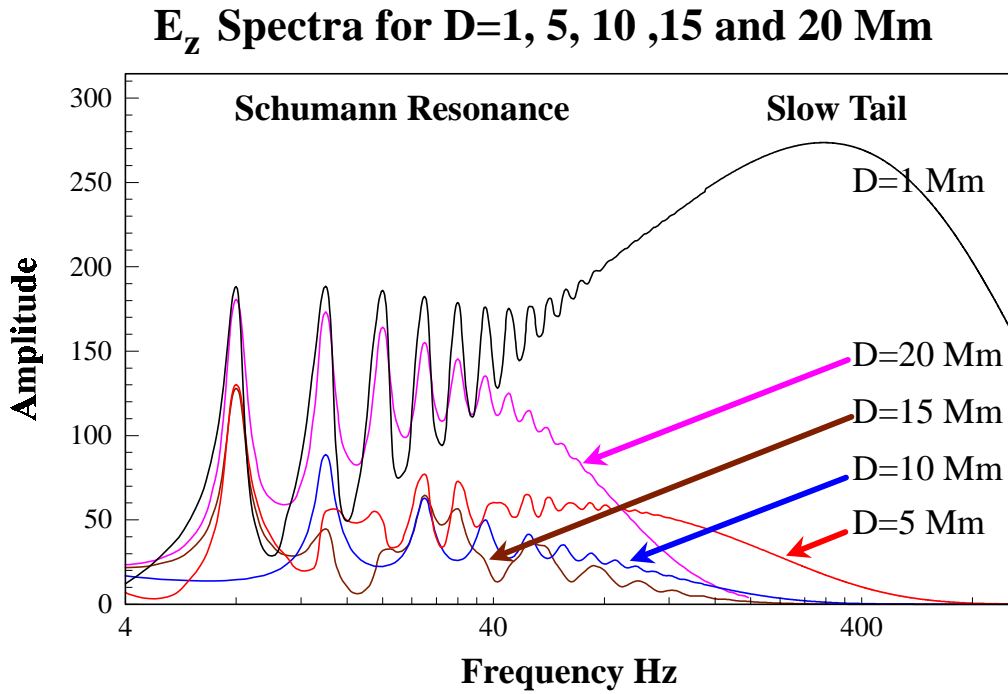

Fig. 2. Samples of the $E_r(f)$ spectra for the source-observer distances $D = 1, 5, 10, 15,$ and 20 Mm.

Fig. 2 presents the samples of the amplitude spectra for the source-observer distances $D = 1, 5, 10, 15,$ and 20 Mm. Frequency varying from 4 to 1000 Hz is plotted along the abscissa in a logarithmic scale. Amplitude of the electric field is shown along the ordinate in $mV/(m \cdot Hz^{1/2})$. The SR peaks are seen at the lower frequencies. Particular form of the resonance pattern depends on the interaction between the direct (source-observer) and antipodal waves. This dependence is used when establishing the source-observer distance (SOD) for the ELF transient events or Q-bursts [11, 20-24].

A broad spectral maximum occupies the frequencies of some hundred Hz when the SOD is relatively small. This is the range of the slow tail atmospherics. As the distance increases, this peak decays due to absorption in the ionosphere that grows with frequency.

To demonstrate the frequency-space distribution of the field amplitude, we apply a shadow contour map of the 'ELF highlands' shown in Fig. 3. Here, the frequency is plotted along the abscissa in the logarithmic scale ($25 \cdot ln\ f$). The source-observer distance D is shown in Mm along the ordinate. The peaks in the amplitude of the vertical

electric field component are seen in the figure casting sharp shadows to the right. The higher a peak is the longer is its shadow.

Two crests (one over the source and another over the source antipode) close a wide valley centered around the 10 Mm distance. There are side transverse ridges descending into the valley that correspond to individual Schumann resonance modes. Each ridge is not smooth, it consists of a series of summits and depressions. Bottom of the valley is not smooth as well, it is covered with a system of regular peaks approaching the antipodal zone. The valley descends and becomes more uniform with the frequency increases. Spectacular feature of Fig. 3 is the system of 'side canyons' that are seen clearly as bright curves, each representing the ELF field nodal line. Such gullies approach the source antipode and form the 'washing board' structure there. The system of canyons corresponds to a family of hyperbolic curves, when a linear frequency scale is applied along the ordinate. A system of equi-distant minima at the 10 Mm distance in the center of the valley is located over the 8, 20, and 32 Hz frequencies relevant to the nodes of odd resonance modes.

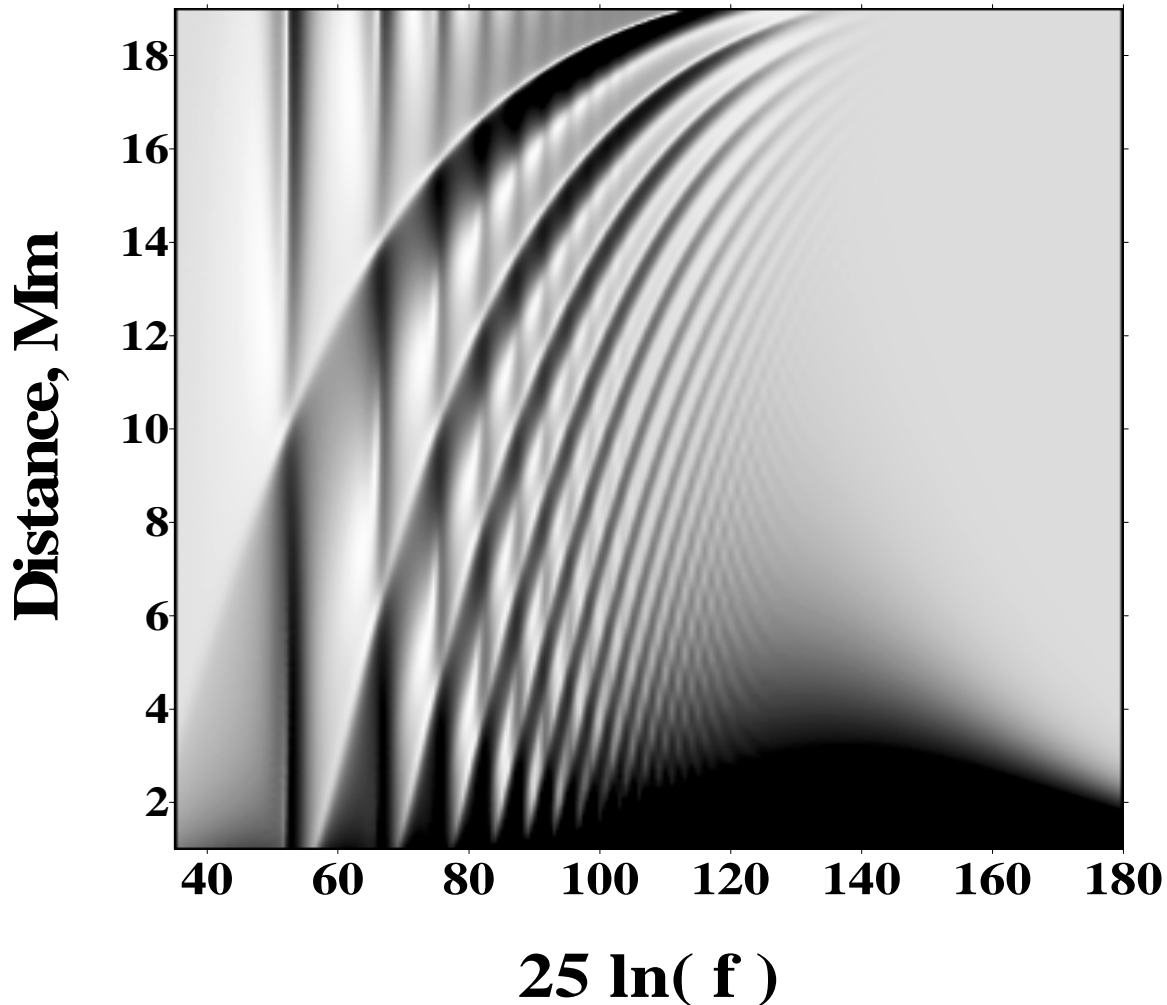# Frequency-Distance Shaded Relief

Fig. 3. Shadow map of the amplitudes of the electric field over the frequency-distance plane.

All the features of the ELF field distribution in the frequency-distance domain including the resonance and antipodal effects are well known. Still, Fig 3 demonstrates the wide-band picture in a rather compact way, emphasising the features never seen in the separate spectral or distance plots, like those shown in Fig. 2.

A comment should be made here concerning the role of the antipodal wave. When a radio signal propagates within a spherical cavity, the shortest distance between the source and observer plays an important role. This is no surprise, since it determines, for instance, the shortest time delay of the EM pulse arriving to the observer. The role of the antipodal path is not so evident. One may say that this is a 'complementary' distance in the spherical cavity, since the direct and antipodal distances form the great circle 40 Mm long. We will see below that these particular arcs lying in the same plane determine two temporal delays of the pulse waves, while the rest of the cavity plays a 'supporting' role.

Actually, the above solution is the Green's function of the problem, since it corresponds to the point delta-source in both the time and space domains. One may easily extend the results for the case of an arbitrary source spectrum using the convolution theorem.

We obtained the waveforms of electric field after applying a FFT procedure to the spectral data. Fig. 4 depicts samples of the $E(t)$ pulse signal computed for 1, 5, 10, 15, and 20 Mm distances. Time in ms is plotted along the abscissa with $t=0$ corresponding to the moment, when the delta-discharge occurs at the source. The figure consists of two frames to compensate for great change in the pulse amplitude that vary from 4 to 0.2 mV/m depending on the distance.

Pulses for relatively short SOD are shown in the upper frame. Amplitude for D=1 Mm is plotted along the left ordinate, while amplitude for D=5 Mm is shown along right ordinate.
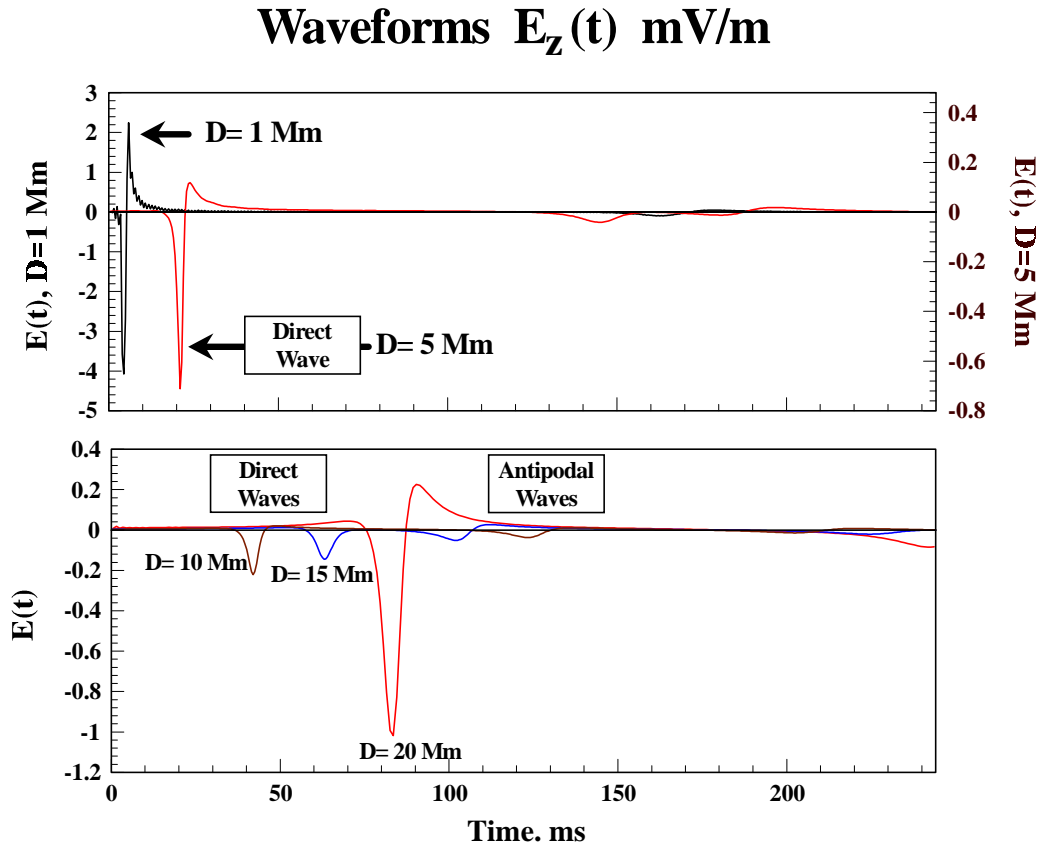
Waveforms $E_z(t)$ mV/m

Fig. 4. Samples of the vertical electric field waveforms at 1, 5, 15 20 Mm distances from the delta-pulse source.

The direct waves reaches the observer with a delay proportional to the distance. Pulses arriving from the source antipode grow as the distance increases. Weakness of the antipodal pulse for the 1 Mm SOD is no surprise, since the electromagnetic power is concentrated at higher frequencies (see Fig.3 and Fig.4). Amplitude of a direct pulse is large at small SOD, and the pulse itself is short. When the SOD grows, the Earth-ionosphere waveguide works as a low pass filter, and higher frequencies attenuate rapidly. The direct pulse becomes smaller, and its width grows. Simultaneously, amplitude of the antipodal wave increases and the relevant pulse becomes noticeable. Direct and antipodal waves tend to become equal when the SOD grows and coalesce in one pulse at the source antipode D=20 Mm.

Here, we consider a single zero-order mode that propagates in the Earth-ionosphere duct from a point delta-source. Fig. 4 shows the waveform evolution that is controlled by the mere $v(f)$ dependence pertinent to the guiding system. When one applies a low-pass filter to observe the Schumann resonance, the amplitude of the direct pulse decreases at short distances and the ratio between the direct and antipode waves increases enabling the global location of the pulse source [11, 17, 20-23].
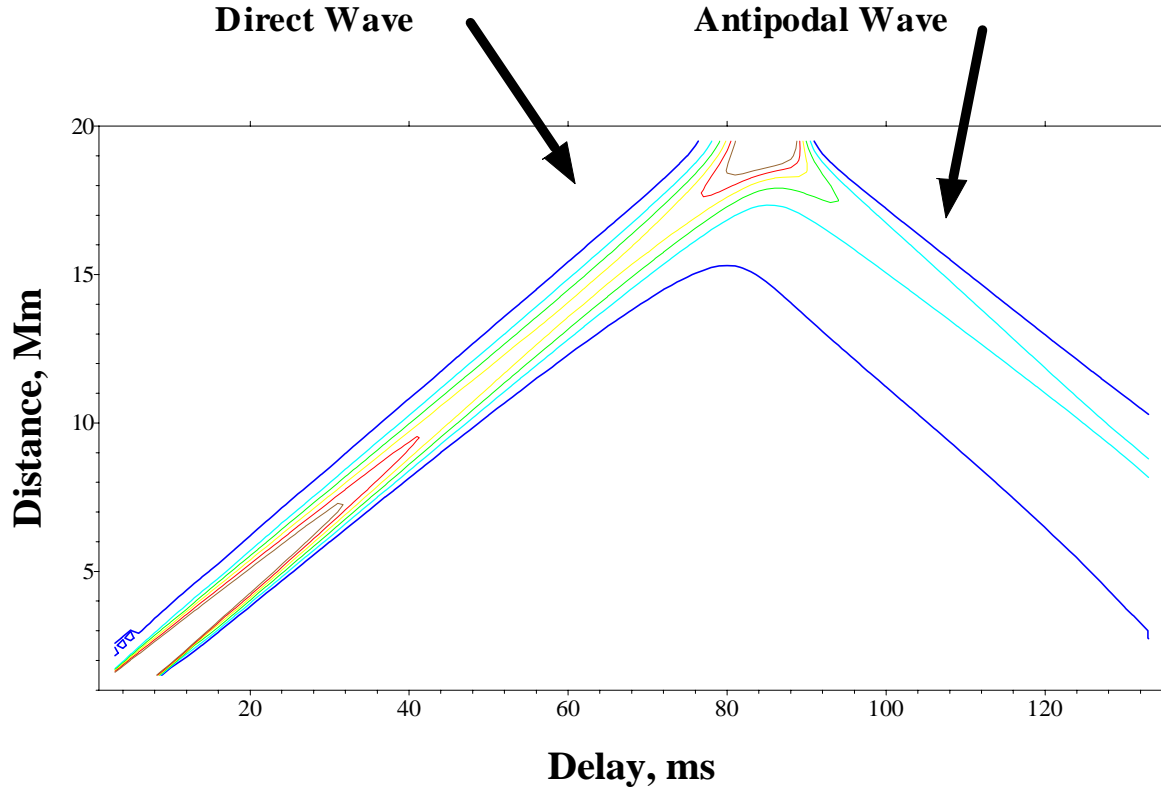
Pulse Bouncing from the Source Antipode

Fig. 5. ELF pulse over the delay-distance plane. Pulse widening and its bouncing from the source antipode are seen.

The 'plane geometry' pertinent to the direct and antipode waves is shown in Fig. 5. Here we plot the contour map of the $E_r(t)$ field component above the delay-distance plane. One has to admit that the ELF radio wave

propagation within a spherical cavity occurs along two great circle arcs: direct and antipodal paths. A 'perfect' reflection of the pulse is seen from the source antipode. Influence of the spherical geometry plays only the role of modifying the pulse amplitudes versus the SOD, e.g. antipodal enhancement of the field.

Fig. 6 demonstrates the pulse amplitude versus the source distance. The whole propagation path length (the circumference of the globe) is shown along the horizontal axis, and the pulse amplitude is plotted along the ordinate in logarithmic scale. The range dependence of the pulse amplitude is shown with dots. When D 'exceeds' the 20 Mm distance the corresponding dot in Fig. 6 shows the amplitude of relevant antipodal wave. For instance, for the 5 Mm source-observer distance we have two pulses: amplitude of the direct wave is plotted at 5 Mm distance, and that of antipodal wave is depicted against the propagation path 35 Mm long.
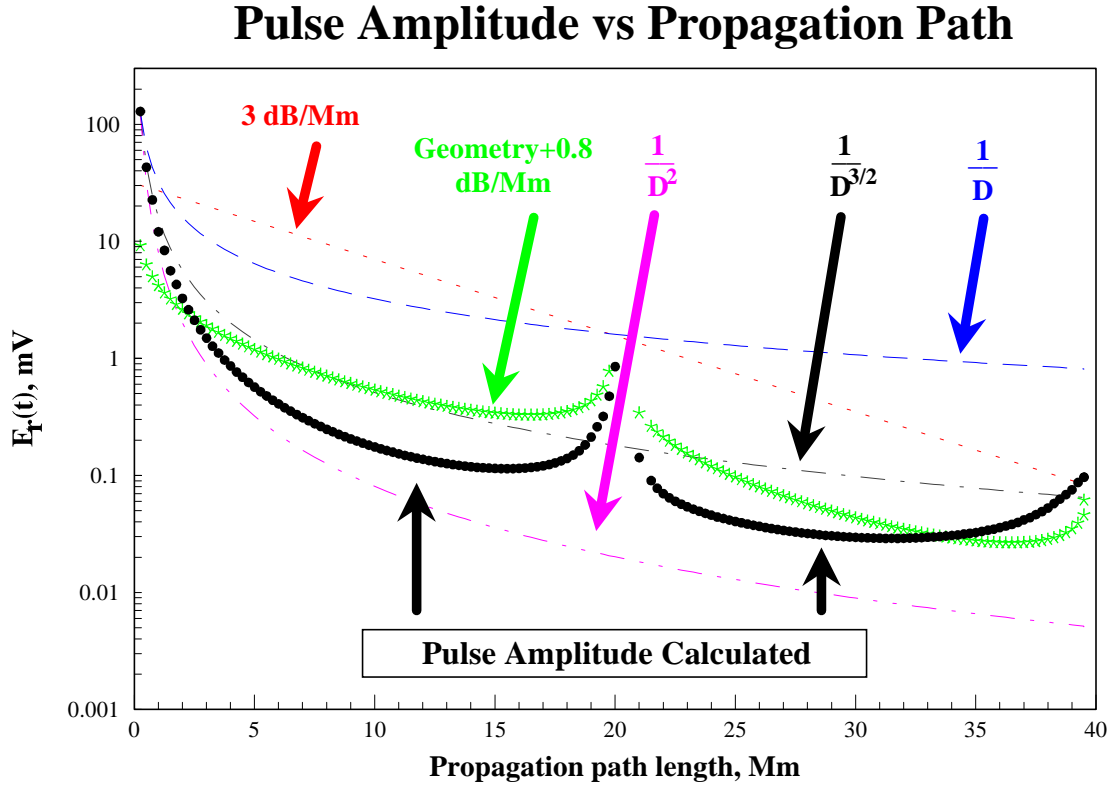

Fig.6. Distance variation of the slow tail amplitude

Sphericity of the guiding system shows itself in the field amplitude. Geometrical enhancement of the field around the source and antipode has been discussed for a long time in the literature. We show additional lines in the plot to compare our results with 'approximating' amplitude variations often used for monochromatic signals. An exponential attenuation of 3 dB/Mm for the plane wave predicts the amplitudes that vary in a linear way within the co-ordinate system applied. The inverse distance dependencies fit the pulse amplitudes in a better way (especially the $1/D^{3/2}$ function) but these have nothing to do with the field enhancement around the source and its antipode. The asterisks in Fig. 6 show the results calculated for a classical narrow band representation of the field (see [7,9,10]), when one accounts for both the attenuation (0.8 dB/Mm) and the focusing. In this case, the field varies as

$$\exp\{-\alpha\theta\}/(\sin\theta)^{1/2}.$$

Fig.6 demonstrates how far the simplified distance dependencies are from the broad-band pulse amplitude. The reason lies in the spectra modifications that occur for the real signal when source-observer distance varies. Meanwhile, the pulse delay depends on the pure geodetic distances between the source, observer and the source antipode (see Fig. 6). It varies in a linear fashion with the SOD. The width of negative and positive half-waves of the pulse varies with the source distance in similar fashion. The effect of the pulse widening is well-known and is applied when establishing the distance from the nearby sources of the slow-tail atmospherics.

Returning to the spectral representation of the ELF signal (Fig. 3 and 4), we must remind that at short source-observer distances the electromagnetic power is concentrated in the range from some hundred to a few thousand Hz. This enables location of the parent discharges when applying the electric antennas with the low input impedance pre-amplifiers that provide a lower cut-off around 200-300 Hz frequency.

To conclude the paper we have presented the main results.

1. Relief of the natural pulse signal over the frequency-distance plane resembles the 'ELF highlands' having regular ridges, peaks and depressions. Peaks and depressions form the chain structures extended over hyperbolic lines over the frequency-distance plane. The relevant lines become the straight over the distance-period plane.
2. The electromagnetic power is concentrated over higher extremely low frequencies (some hundred Hz) when the source-observer distance is small. This explains an effectiveness of the nearby source location using the slow tail atmospherics. Beginning from some Mm distance, the 'high frequency' component becomes completely absorbed by the lower ionosphere, and the energy shifts into the SR band. This is why the Schumann resonance supports the global location of the powerful lightning discharges.
3. Radio pulse moves with a constant velocity in the time domain. A 'bouncing' occurs in the time domain from the source antipode (and the source itself). The pulse width grows monotonously with the propagation path length.
4. The distance dependence of the natural wide band pulse amplitude is conditioned by two factors. The first is the field focusing around the source and the source antipode due to spherical geometry of the guiding system. The second is the spectra modifications due to absorption in the ionosphere. Attenuation of the higher frequencies governs the dependence of a pulse amplitude versus propagation distance.

1. *Lyons, W.A.* Characteristics of luminous structures in the stratosphere above thunderstorm imaged by low-light video // Geophys. Res. Letters. - 1994. - **21**, P.875-878.
2. *Sentman, D.D., Westcott E.M.*, Observations of upper atmosphere optical flashes recorded from an aircraft // Geophys. Res. Letters. - 1993. - **20**, P.2857-2860.
3. *Sentman, D.D., Westcott E.M., Osborne D.L., Hampton D.L., Heavner M.J.*, Preliminary results from the Sprites 94 aircraft campaign // Geophys. Res. Letters. - 1995. - **22**, P.1205-1208.
4. *Boccippio, D.J., Williams E.R., Lyons W.A., Baker I., Boldi R.*, Sprites, ELF transients and positive ground strokes // Science. - 1995. - **269**, P.1088-1091.
5. *Sukhorukov, A.I., Stubbe P.*, On ELF pulses from remote lightning triggering sprites // Geophys. Res. Letters. - 1997. - **24**, P.1639-1642.
6. *Nickolaenko, A.P., Rafalsky V.A.*, Power spectra of the transverse resonances in the Earth-ionosphere cavity // Izvestija VUZov Radiofizika, **26**, 1059-1064, 1983.
7. *Wait, J.R.*, Electromagnetic waves in stratified media. - Oxford, New York, Paris: Pergamon Press, 1962. - 463p.
8. *Galejs, J.,* Terrestrial propagation on long electromagnetic waves, Oxford, New York, Paris: Pergamon Press, 1972. - 398 p.
9. *Bliokh, P.V., Nickolaenko A.P., Filippov Yu.F.*, Global electromagnetic resonances in the Earth-ionosphere cavity. Naukova Dumka Kiev, 1977, 199 p.
10. *Makarov, G.I., Novikov V.V., Rybachek S.T.*, Propagation of the radio waves in the Earth-ionosphere guiding system, Nauka, Moscow, 1994, 152 p.
11. *Nickolaenko, A.P., Kudintseva I.G.*, A modified technique to locate the sources of ELF transient events // J. Atmos. Terr. Phys. - 1994. **56**, P.1493-1498.
12. *Nickolaenko, A.P.*, ELF/VLF propagation measurements in the Atlantic during 1989 // J. Atmos. Terr. Phys. - 1995. **57**, P.821-831.
13. *Nickolaenko, A.P.*, Modern aspects of Schumann resonance studies // J. Atmos. Solar-Terr. Phys. - 1997. **59**, P.805-816.

14. *Greifinger, C. Greifinger P.*, Approximate method for determine ELF eigenvalues in the Earth-ionosphere waveguide // Radio Sci. - 1978. - **13**, P.831-841.
15. *Nickolaenko, A.P., Rabinowicz L.M.*, On the possibility of the global electromagnetic resonances on the planets of Solar system // Kosmicheskie Issledovasniya, **20**, 82-87, 1982.
16. *Sentman D.D.*, Approximate Schumann resonance parameters for a two-scale -height ionosphere // J. Atmos. Terr. Phys. - 1990. **52**, P.35-47.
17. *Bliokh, P.V., Nickolaenko A.P., Filippov Yu.F.*, Schumann resonances in the Earth-ionosphere cavity, /D.Ll. Jones-ed., Peter Perigrinus, Oxford, New York, Paris, 1980, 168 pp.
18. *Nickolaenko, A.P., Rabinowicz L.M.*, Speeding up the convergence of zonal harmonic series representation in the Schumann resonance problem // J. Atmos. Terr. Phys. - 1995. **34**, P.979-985.
19. *Jones, D. Ll., Burke C.P.*, Zonal harmonic series expansions of Legendre functions and associated Legendre functions, J. Phys. A. Math. Gen. - 1990. **23**, P.3159-3168.
20. *Kemp, D.T., Jones D. Ll.*, A new technique for analysis of transient ELF electromagnetic disturbances within the Earth- ionosphere cavity // J. Atmos. Terr. Phys. - 1971. **33**, P.567-572.
21. *Kemp, D.T.* The global location of large lightning discharges from single station observations of ELF disturbances in the Earth- ionosphere cavity // J. Atmos. Terr. Phys. - 1971. **33**, P.919-928.
22. *Burke, C.P., Jones D. Ll.*, An experimental investigation of ELF attenuation rates in the Earth-ionosphere duct // J. Atmos. Terr. Phys. - 1992. **54**, P.243-254.
23. *Burke, C.P., Jones D. Ll.*, On the polarity and continuous currents in unusually large lightning flashes deduced from ELF events // J. Atmos. Terr. Phys. - 1996. **58**, P.531-540.
24. *Sentman D.D.*, Schumann Resonances, Handbook of atmospheric electrodynamics //H. Volland-ed., Atmospheric electricity. - London, Tokyo: CRC Press Inc., Boca Raton, 1995.- 1. P.267-298.
25. *Sentman D.D.*, Long baseline observations of Schumann resonance, Abstracts of reports at IUGG XXI General Assembly, Boulder, Colorado, July2-14 1995, MA22C-08. 1995, P.A280.